ISSN NO. 2320-5407

Journal homepage: http://www.journalijar.com

INTERNATIONAL JOURNAL OF ADVANCED RESEARCH

RESEARCH ARTICLE

SYNTHESIS OF NOVEL CERIUM DOPED POLYANILINE MULTIWALLED CARBON NANOTUBES AND THEIR OPTICAL AND ELECTROCHEMICAL PROPERTIES FOR SUPERCAPACITOR APPLICATIONS

S. Tharani, S. Chidambara Vinayagam*
Department of Chemistry, Presidency College, Chennai-600 005.

Manuscript Info

Manuscript History:

Received: 15 January 2015
Final Accepted: 25 February 2015
Published Online: March 2015

Key words:

Multiwalled carbon nanotubes, Polyaniline, Specific capacitance, Photoluminescence.

Corresponding Author

S. Chithambara Vinayagam

Abstract

PANI/$Ce(NO_3)_3$/MWCNTs nanocomposites are synthesized *via* in situ oxidative polymerization of aniline monomer in HCl solution. The PANI/$Ce(NO_3)_3$ was homogeneously coated on the surface of MWCNTs which greatly improved the charge transfer reaction. The PANI/$Ce(NO_3)_3$/ MWCNTs nanocomposites exhibit better electrochemical performances than that of neat individual components. The maximum specific capacitance of 900 Fg^{-1} was obtained at a scan rate of 5 mVs^{-1} for PANI/5 wt% $Ce(NO_3)_3$ composite with 7 wt% MWCNT, compared to 210, 350, 564, and 740 Fg^{-1} for neat PANI, PANI/5 wt% $Ce(NO_3)_3$, PANI/5 wt% $Ce(NO_3)_3$/3 wt% MWCNT and PANI/5 wt% $Ce(NO_3)_3$/5 wt% MWCNT, respectively. The combination of electron donating PANI and cerium semiconductor enhanced both the electron mobility in the nanocomposites and photoluminescence behavior. The relatively PL was achieved with higher weight % of MWCNT as the excimer quenching by MWCNT was shielded a PANI coat. The resulting composite can use as promising electrode materials for high performance electrical energy storage devices.

INTRODUCTION

Supercapacitors have played an increasingly important role in applications such as the auxiliary power source in combination with battery in hybrid electric vehicles, short-time power source for mobile electronic devices, backup power sources for computer memory *etc*. [Arbizzani *et al*., 1997; Conway, 1991; Conway, 1999; Kotz and Carlen, 2000; Otero, 1999]. In recent years, a lot of research interest was focused on conducting polymer based supercapacitors owing to their high capacitive characteristics and low material cost. Among numerous conductive polymers, polyaniline (PANI) is considerably attractive because of its easy synthesis, low cost, environmental stability, high and controllable conductivity [Li *et al*., 2002; Ryu *et al*., 2002]. Generally, polymers are lack of extended π conjugation, which is the main criteria for the electrical conductivity, but organic polymers such as PANI, polypyrrole *etc*. have extended π bonds thus act as conducting materials by the carrying the charge along the chain. $IrCl_3$ polypyrrole gives enhanced capacitance for electrochemical energy storage device, $RuCl_3$ doped polypyrrole gives higher capacitance in $NaNO_3$ electrolyte solution, $MnCl_2$ doped polyaniline was also used for electrochemical supercapacitor application and gives 474 Fg^{-1} with highest doping level [Cong *et al*., 2013; Patil *et al*., 2011; Wang *et al*., 2013; Yuan *et al*., 2012]. However, a low cycle life and poor mechanical properties, resulting from the swelling and shrinkage during the doping/dedoping processes limit its application as individual electrode material. In order to alleviate the limitation, composites of PANI/carbon materials (e.g. graphene carbon nanotubes (CNTs), [Chen *et al*., 2010; Iranagh *et al*., 2013; Ni *et al*., 2010]), and PANI/inorganic oxides (e.g. MnO_2, SnO_2, TiO_2, [Ben *et al*., 2004; Bian *et al*., 2009; Chi *et al*., 2000; Hu *et al*., 2009; Xie *et al*., 2014]) have been proved

to be attractive to reinforce the stability of PANI as well as maximize the capacitance value. Transition metal oxides are considered to be the most suitable candidate materials for electrochemical capacitors. These stem from the high specific capacitance coupled with low resistance resulting in a high specific power which makes them suitable for commercial applications. For example, many researchers have investigated transition metal doped conducting polymer and have found higher conductivity with increase in doping level of transition metal. More importantly, CNT is an excellent support material due to its high surface area, which can promote the active materials evenly dispersed on its surface and fast electron transfer; thus, improving the utilization of active materials.

Most recently, to get the electrode materials with better electrochemical performance, various ternary composites have gained much attention. Yu *et al*., (2012) have reported the fabrication of graphene/MnO_2/CNT composite by 3D conductive wrapping of graphene/MnO_2 with CNTs. Han *et al*., (2014) have prepared MnO_2 nanorods intercalating graphene oxide/PANI ternary composites. Those ternary composites both showed better electrochemical performance than the corresponding binary composites. However, until now, studies about graphene/MnO_2/PANI ternary composite are still limited. Researches indicate that electrochemical characteristics of electrode materials are highly dependent on the grain size, texture, surface area and morphology [Xu *et al*., 2006]. The unique nanostructures, such as nanotube or nanorod arrays, nano network and porous structure [Li *et al*., 2012; Lee *et al*., 2013; Ozkazanc *et al*., 2012; Wang *et al*., 2013; Yu *et al*., 2011] are very conductive to improving the electrochemical characteristics of electrode materials. To the best of knowledge, the limited reports only available on the investigation of lanthanide ions doped nanocomposites as electrode material. Doping of rare earth metals has received great attention due to its peculiar, optical and catalytic properties arising from the accessibility of shielded 4f levels. In this research work, we have synthesized Ce^{3+} ion doped PANI using cerium nitrate as nanocomposites by using MWCNTs. Cerium ion have strong binding affinity with the nitrogen lone pair of PANI, which improve the stability of electrode material and increase the cyclic stability, and also doping of cerium ions in the polymer matrix influence the particle size, acts as a redox active catalyst and significantly increase the absorbance property.

2. Experimental

2.1. Materials

Aniline was distilled under the protection of high purity N_2, and then kept in a refrigerator before use. All the other chemicals were analytical reagent, and used without further purification. Multiwall carbon nanotubes (MWCNT, diameter of 40–50 nm and length of 50 μM) were purchased from Sigma Aldrich. Ammonium persulphate and hydrochloric acid were purchased from SD Fine chemicals, India. Cetyltrimethylammonium bromide (CTAB) was purchased from Sigma Aldrich, USA.

2.2. Instrumentation

The Fourier transform-infrared (FT-IR) spectra were recorded on a Perkin Elmer 100 FT-IR spectrometer. Solid samples were embedded in KBr disc. The field emission scanning electron microscopy (FE-SEM) used in this work was done using a NanoSem 230 microscope. Ultraviolet-Visible (UV-Vis) spectra were obtained on a Varian Cary 5000 UV-Vis spectrometer. Stock solutions were prepared by dissolving 10 mg of each sample in 1 L of N-methyl-2-pyrrolidone (NMP). Photoluminescence (PL) measurements were performed using a Varian Cary Eclipse Fluorescence Spectrometer. The excitation wavelength was that of the UV absorption maximum of each sample. Powder X-ray diffraction patterns were recorded at room temperature by monitoring the diffraction angle 2θ from 10 to 70° as the standard on a Rich Siefert (Model 3000) X-ray powder diffractometer. Thermo gravimeter analysis was carried out using the DSTA 409 PC analyzer (Netzsch Gerateban GmbH). For electrochemical measurements, cyclic voltammetry (CV) was carried out using a Versa STAT3 AMETEK Model (Princeton Applied Research, USA) potentiostat/galvanostat employing a standard three electrode electrochemical cell. This consisted of samples on glassy carbon (GC) with a diameter of 3 mm as the working electrode, Ag/AgCl reference electrode and platinum gauze as the counter electrode. Experiments were carried out at room temperature in 0.1 M H_2SO_4 electrolyte solution. Nitrogen gas was used to purge the solution to achieve an oxygen-free electrolyte solution. All potentials are reported relative to Ag/AgCl (in saturated KCl) reference electrode recorded at a scan rate of 5 mVs^{-1}. The potential window for cycling was confined between −0.2 V and +1.0 V in acidic electrolyte. The GC electrode was polished with alumina slurry prior to use to obtain a mirror-like surface. Samples (2.0 mg) were dispersed in NMP (0.2 mL) and aliquots of the suspension (10 μL) were coated on GC electrodes and dried under reduced pressure (0.5 mmHg) for 24 h at 50 °C. Nafion (5%, 5 μL) in ethanol was pipetted onto the sample/GC electrode and allowed to dry at laboratory conditions for 2 h.

2.3. Synthesis of polymer nanocomposites

Initially the effect of cerium on pure PANI was studied with varying the weight (wt) % of cerium nitrate by 1, 3 and 5 wt%, respectively. We arrived to a conclusion that 5 wt% cerium nitrate doped PANI exhibited better absorption as well as emission properties. So in order to achieve emission as well as supercapacitance in the

composite, we extended our work in studying the doping effect of MWCNT (1–7 wt%) in the 5 wt% $Ce(NO_3)_3$ doped PANI. Aniline was stirred in 150 mL 1 M HCl and then 5 wt% cerium nitrate was added to the above mixture and stirred for 30 min. In another beaker, calculated weight percentage of MWCNT and CTAB was sonicated in 1 M HCl in order to avoid agglomeration of MWCNTs. To this MWCNT solution, aniline and cerium nitrate mixture was added and maintained in ultra sonication for 30 min. Then ammonium persulfate (APS, 2.5 mmol) in 30 mL of 1 M HCl solution was slowly added drop by drop into the above mixture with constant stirring. Polymerization of aniline started after about 5 min, and then the reaction was allowed to stir overnight. The mixture was diluted by 200 mL of deionized water. The precipitated composite was collected by filtration, and repetitively washed with water and ethanol until the filtrate became colorless, dried at 60 °C for 12 h in a vacuum oven. A proposed mechanism of PANI/$Ce(NO_3)_3$/MWCNTs nanocomposite formation is depicted in **Scheme 1**. For comparison, pure PANI was also synthesized through the aforesaid chemical process without the presence of MWCNT suspension. After having been dried under vacuum at 60 °C for 12 h, the PANI powder was obtained.

3. Results and discussion

3.1. Infrared spectral analysis

The FT-IR spectra of the PANI, PANI/5 wt% $Ce(NO_3)_3$ and PANI/5 wt% $Ce(NO_3)_3$/1–7 wt% MWCNTs nanocomposites are shown in **Fig. 1**. The characteristic IR bands of pure conducting emeraldine salt form of PANI (**Fig. 1a**) were observed at 787 cm^{-1} (C−H stretching), 1100 cm^{-1} (C−H bending), 1238 cm^{-1} (C−N stretching mode for quinoid units), 1292 cm^{-1} (C=N stretching mode), 1384 cm^{-1} (C=N stretching mode for quinoid units), 1460 cm^{-1} (C−C stretching of the benzenoid ring) and 1560 cm^{-1} (C=C stretching of the quinoid ring). The peak at 3450 cm^{-1} (N−H stretching mode) was observed for only undoped and 1 wt% cerium nitrate doped PANI (**Fig. 1b**). In addition, the intensity of the peak at 3450 cm^{-1} referring to N–H stretching mode almost disappears at 3 wt% and 5 wt% doping levels of cerium nitrate (**Fig. 1c** & **1d**) [Markovic *et al*., 2006]. This was due to the interaction between the nitrogen atoms in the polymer chain and cerium ions. Some of the peaks have also shifted due to the effects of the doping process. The IR spectra of PANI/$Ce(NO_3)_3$/MWCNTs nanocomposites (**Fig. 1e** & **1f**) showed a higher intensity ratio between 1586 cm^{-1} and 1499 cm^{-1} than neat PANI, endorsing the presence of strong interactions between MWCNT and the quinonoid units of PANI [Saini *et al*., 2009].

3.2. Raman spectral analysis

Raman spectrum of pure PANI (**Fig. 2a**) exhibits two characteristic peaks at 1500 cm^{-1} and 1172 cm^{-1} which was assigned to C=N stretching in quinoid units, and C–H bending in benzenoid units, respectively. The peak located at 1588 cm^{-1} correspond to C=C stretching in the quinoid ring. In the Raman spectrum of pure PANI, the broad band centered at 1353 cm^{-1} was associated to the stretching mode of C–N delocalized polaronic structure, which was characteristic of the protonated imine form of polyaniline. Raman spectra show the position of the C–N stretching band was shifted to higher wave number, *i.e*. 1368, 1372 and 1371, respectively, for 1, 5 and 7 wt% MWCNT doped with PANI/5 wt% $Ce(NO_3)_3$ nanocomposites denoted as **Fig. 2b, c** & **d**, respectively. This shifting could be attributed to the electrostatic interaction between the C–N species of PANI matrix and the MWCNT. The G band peak at 1591 cm^{-1} in the base PANI was shifted to 1601 cm^{-1}, 1602 and 1605 cm^{-1}, respectively, with 1, 5 and 7 wt% MWCNT doped with PANI/5 wt% $Ce(NO_3)_3$ nanocomposite and this indicates the strong interaction between MWCNT and PANI/5 wt% $Ce(NO_3)_3$ nanocomposites.

3.3. UV-Vis spectral analysis

Absorption spectroscopy was used to characterize the chemical structures of synthesized PANI/$Ce(NO_3)_3$/ MWCNTs nanocomposites. The electronic absorption spectra of neat PANI, PANI/5 wt% $Ce(NO_3)_3$ and PANI/5 wt% $Ce(NO_3)_3$/MWCNTs nanocomposites are demonstrated in **Fig. 3**. It can be seen that the UV-Vis spectrum of PANI shows two sharp peaks with the maxima at 329 (peak 1) and 624 nm (peak 2). These observed peaks are correspond to π–π* transitions centered on the benzenoid and quinoid units, respectively. The UV spectrum of PANI/$Ce(NO_3)_3$ show the UV absorption edge of π–π* transitions centered on the benzenoid and quinoid units, shifts towards the longer wavelength of 350 and 630 nm, respectively, with 5 wt% $Ce(NO_3)_3$. Adding 1 wt% MWCNT into PANI/$Ce(NO_3)_3$ matrix red shifts the absorption peak of the π–π* transition from 350 (3.5) to 371 nm (3.3 eV) and a blue-shift of the polaron–π* transition from 629.7 (1.96 eV) to 613 nm (2.0 eV) were observed due to the increase in the π conjugation in the PANI/$Ce(NO_3)_3$/MWCNTs backbone [Zengin *et al*., 2002]. With 5 and 7 wt% MWCNT incorporation into PANI/$Ce(NO_3)_3$ matrix blue shifts the absorption peak of the π–π* transition to 326 and 329 nm, respectively. Such a hypsochromic shift of the π–π* band in PANI/$Ce(NO_3)_3$/MWCNTs compared to PANI has been reported in the literature [Gopalan *et al*., 2007; He *et al*., 2001], and it has been suggested to be due to the site-selective interaction between the quinoid ring of the PANI and MWCNTs [Jeevananda *et al*., 2008]. When PANI coats over the MWCNTs, the interfacial interaction between the two causes the π–π* transition to shift

to a lower wavelength [Yang *et al*., 2010]. But at the same time, the absorption peak due to the polaron/bipolaron transition was red shifted in PANI/$Ce(NO_3)_3$ to 639 (1.94 eV) and 640 nm (1.93 eV) with 5 and 7 wt% MWCNT, respectively, compared to that of neat PANI. This red shift in peak may be assigned to the site selective interaction between MWCNT and quinoid ring structure of ES, facilitating charge transfer.

3.4. Powder XRD analysis

The powder XRD patterns of neat PANI, PANI doped with 5 wt% $Ce(NO_3)_3$ and PANI/5 wt% $Ce(NO_3)_3$ with different wt% (1, 3, 5 and 7 wt%) MWCNTs are depicted in **Fig. 4**. The PANI/$Ce(NO_3)_3$/MWCNTs nanocomposites show different XRD patterns with a broad scattering at 2θ values between 10° and 30°. PANI exhibits XRD pattern corresponding to 2θ = 16°, 18° and 25° [Cochet *et al*., 2001] indicates the amorphous state of PANI. As the cerium was incorporated in the polymer matrix, sharpened distinct peak of XRD pattern was found, which inferred the development of crystallinity in the nanocomposites. When the wt% of MWCNTs was increased (3, 5 and 7 wt%) then the increased intensities of the nanocomposites were also observed which clearly explain the crystalline nature of the composites.

3.5. Surface morphological analysis

The formation mechanism of PANI/$Ce(NO_3)_3$/MWCNTs nanocomposites was believed to involve electrostatic interaction between PANI and MWCNTs. The surface morphology of pure PANI, PANI/5 wt% $Ce(NO_3)_3$ and PANI/5 wt% $Ce(NO_3)_3$/1–7 wt% MWCNTs nanocomposites was analyzed from SEM micrographs, as presented in **Fig. 5**. As shown in figure, the pure PANI morphology is coalesced, making the surface rough with no uniformity. Due to doping of $Ce(NO_3)_3$, a secondary phase is present and it is highlighted by arrows having a flaky morphology occurring in the matrix is with brighter contrast. This phase is more visible in the 5 wt% $Ce(NO_3)_3$/PANI composite. The structure is relatively more homogeneous and the interaction between the particles and the matrix is stronger. Micro-structural differences seen in PANI and its nanocomposites with respect to particle structures and secondary phase are expected to affect their absorption, emission and electrochemical behavior. However the morphology of PANI film has been changed by the introduction of MWCNT as shown in **Fig. 5** (**d-f**). The well-dispersed MWCNT fibers may serve as condensation nuclei during the growth process of PANI and therefore they were coated with a considerable amount PANI to form such a fiber materials which may give rise to conductive pass ways. The sorption of the aniline monomer onto MWCNTs is possible because of its high surface area [Cochet *et al*., 2001; Jeevananda *et al*., 2008], and the sorbed monomer then polymerizes on MWCNT to form PANI-coated MWCNTs. The PANI/5 wt% $Ce(NO_3)_3$/MWCNTs phase formed a core-shell structure with an average diameter in the range of 100–240 nm, much larger than that of MWCNT whose diameter was about 50 nm. The SEM micrographs also clearly reveal the wrapping by PANI onto the MWCNT template, and show a significant increase in the diameter of the MWCNTs after composite formation. As the weight percentage of MWCNT was increased by 1, 5 and 7 wt%, which is indicative of the thickness of PANI layer coated on the MWCNTs. These micro-structural variations also impose a profound influence on the resulting capacitive behavior of the PANI/5 wt% $Ce(NO_3)_3$/MWCNTs nanocomposites. This is because, MWCNTs are relatively good electron acceptors while PANI may be considered to be a good electron donor [Ghatak *et al*., 2010]. This can facilitate the π–π* interaction between the surface of MWCNT and the quinonoid rings of polyaniline, and this helps the MWCNT configure into a three dimensional network structure which is very conductive to escalate the chance of interaction between the PANI and the electrolyte, which can increase more active sites of the composite films for faradaic reaction and larger SC than pure PANI film. As seen in **Fig. 6**, cerium ion is present in the EDX plot, which is an indication for successful incorporation of metal oxide in the nanocomposites structure.

3.6. Photoluminescence spectral analysis

The luminescent properties of pristine PANI and PANI/5 wt% $Ce(NO_3)_3$/MWCNTs nanocomposites are shown in **Fig. 7**. The photoluminescence spectrum of PANI shows a peak at 465 nm and the intensity has increased enormously in blue region of visible spectrum, due to the formation of more density of states in the energy band upon the addition of cerium. The electronic configuration of cerium (Z= 58) is [Xenon] $4f^2\ 5d^0\ 6s^2$ with $2F_j$ its ground state. When cerium is doped into a PANI its ground state splits into $2F_{5/2}$ and $2F_{7/2}$ sub-levels and its excited state splits into five components. The inner orbit 4f is shielded from the ligand field by the closed 5s and 5p orbital so it is less affected by the ligand field. However, the excited state orbital 5d is close to the outer field, so it interacts strongly with the outer field. As a result of which the 4f–4f transition is narrow when compared to 5d–4f transition [Ghatak *et al*., 2010]. Since the separation between 4f and 5d energy level is large, 5d to 4f transition will be radio-active. Hence peaks at 463 and 473 nm are ascribed due to lowest level of 5d to ground sublevels *i.e.* $5d \rightarrow 2F_{7/2}$ and $2F_{5/2}$. Therefore the emission most probably comes from the lowest 5d to 4f levels of Ce^{3+} ion. This is the electric dipole allowed transition and gives strong emission in blue region. Because of the combination of electron donating groups such as NH in PANI, and semiconducting cerium, the electron mobility is enhanced in the nanocomposites. This favors the formation for singlet exciton, which decays radiatively to the ground state resulting in enhanced

PL. The emission maxima of PANI/5 wt% $Ce(NO_3)_3$/MWCNTs were at around 470–476 nm. The peak intensity of 1, 3 and 5 wt% MWCNT doped with PANI/5 wt% $Ce(NO_3)_3$ nanocomposites was higher than that of PANI and this behavior was quite contradictory in the presence of MWCNT because MWCNTs are strong excimer quenchers and light absorbers [Battcharya *et al*., 2013]; if MWCNTs/PANI were physically aggregated by intermolecular interactions in the solid state and if they are segregated in solution, the emission intensity of PANI/5 wt% $Ce(NO_3)_3$/MWCNTs would be much weaker. However the relatively higher peak intensity implied that PANI was uniformly covered onto the surface of MWCNT in such a way that the PANI/5 wt% $Ce(NO_3)_3$/MWCNTs excimer quenching by MWCNT was shielded by a PANI coat, and this was clearly evident from the increase in the thickness of the MWCNT obtained from the SEM images.

3.7. TGA analysis

The thermal behaviors of the synthesized nanocomposites neat PANI, PANI/5 wt% $Ce(NO_3)_3$ and PANI/ 5 wt% $Ce(NO_3)_3$ with different wt% of MWCNTs (1–7 wt%) were analyzed by thermogravimetric analysis at nitrogen atmosphere, and the plot of percentage weight loss as a function of temperature is shown in **Fig. 8**. Thermal stability of the nanocomposites is needed for its applications in the supercapacitors as electrode materials. In the TGA analysis, all the nanocomposites found similar behavior, but different thermal stabilities were obtained. On comparing, 5 wt% $Ce(NO_3)_3$ doped PANI with 7 wt % MWCNTs was thermally more stable electrode material among all the nanocomposites, because of the highest wt% of MWCNTs [Nayak *et al*., 2011]. The TGA analysis was conducted from 30–800 °C. The thermal degradation was commenced from 100–150 °C, which was the elimination of H_2O molecules in the nanocomposites. Upto 340 °C no significant residual weight loss was observed, and after 340 °C one of the dopant (C1) was removed. From 350–600 °C, there was a noticeable weight loss for all the nanocomposites where the breaking of carbon skeleton was found, and at 600 °C it reached to be maxima. After 600 °C a constant line was shows by all the nanocomposites [Reisfeld *et al*., 1998]. The increased stability of the PANI/5 wt% $Ce(NO_3)_3$/MWCNTs nanocomposites over that of MWCNTs/PANI is likely to be results of strong coordination among all the constituents. From the analysis, it was concluded that these nanocomposites were thermally more stable, encouraging and suitable electrode materials for supercapacitor applications.

3.8. Electrochemical properties

Electrochemical characterization of the synthesized nanocomposites was carried out to explore their potential application as active material for supercapacitor electrodes. The cyclic voltammogram for the PANI/5 wt% $Ce(NO_3)_3$/MWCNTs nanocomposite electrode at scan rate of 5 mV/s (**Fig. 9**). Peaks of C1/A1 are ascribed to the redox transition of PANI from a semiconducting state (leuco-emeraldine form) to a conducting state (emeraldine form) and Faradaic transformation from emeraldine to pernigraniline is responsible for peaks of C2/A2 [Choi *et al*., 2011; Fusalba *et al*., 2001; Rudge *et al*., 1994]. The increase in the redox species encourages strong interaction between the aromatic structures of MWCNT and ES, and favors the uncoiling of PANI chains. In this uncoiled conformation, the probability of moieties exposed for oxidation is more leading to higher Faradaic current. The specific capacitance of 900 Fg^{-1} is recorded maximum for 5 wt% $Ce(NO_3)_3$/PANI composite with 7 wt% MWCNT, compared to that of neat PANI which is 210 Fg^{-1} and 350, 564 and 740 Fg^{-1} for 1, 3 and 5 wt% of MWCNTs, respectively. The superior specific capacitance is attributed to the strong interaction of large bonded surface of MWCNTs with the conjugated structure of PANI *via* π-π stacking, and thus the highly conjugated system has promoted the degree of electron delocalization and preferential protonation of the amine nitrogen atoms [Huang *et al*., 2003; Wang *et al*., 2006].

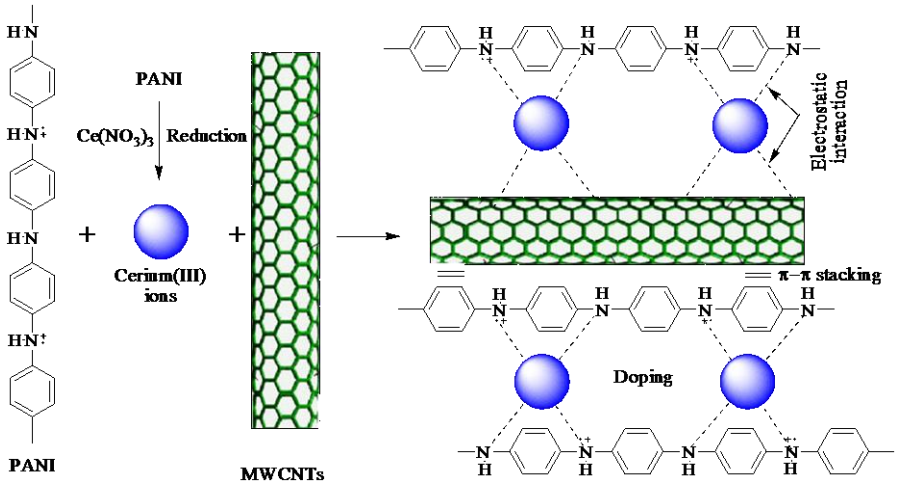

Scheme 1: A proposed mechanism of PANI/5 wt% $Ce(NO_3)_3$/MWCNTs nanocomposite formation

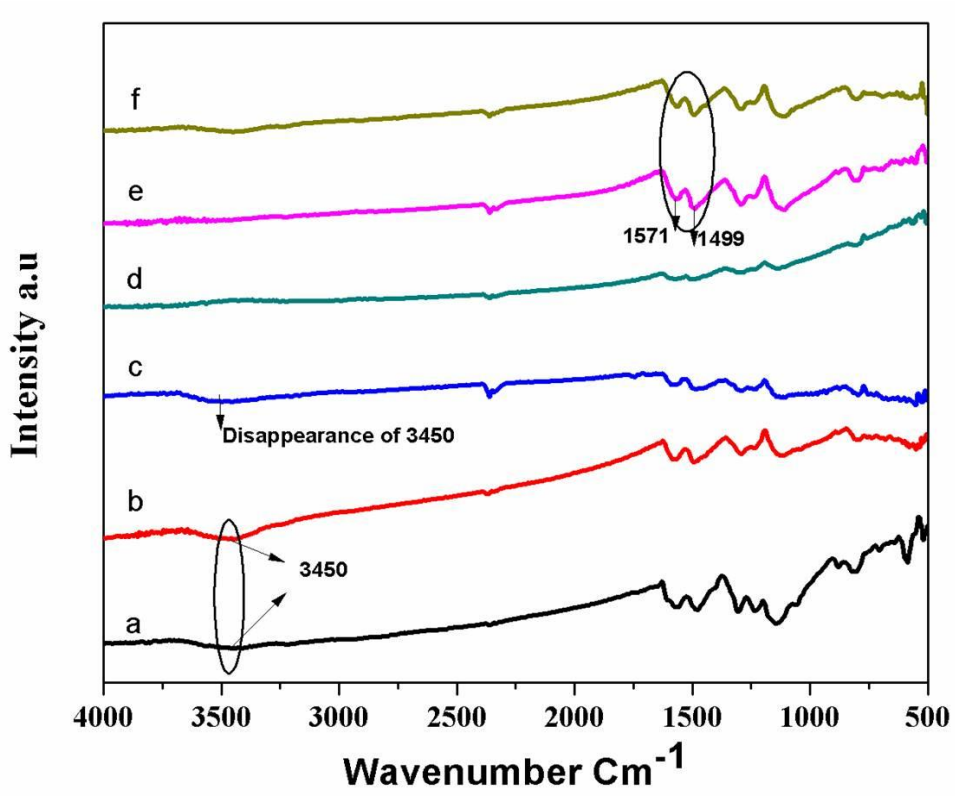

Figure 1: FT-IR spectra of nanocomposites neat PANI (a), PANI/5 wt% $Ce(NO_3)_3$ (b), PANI/5 wt% $Ce(NO_3)_3$/ 1 wt% MWCNTs (c), PANI/5 wt% $Ce(NO_3)_3$/3 wt% MWCNTs (d), PANI/5 wt% $Ce(NO_3)_3$/5 wt% MWCNTs (e) and PANI/5 wt% $Ce(NO_3)_3$/7 wt% MWCNTs nanocomposites (f)

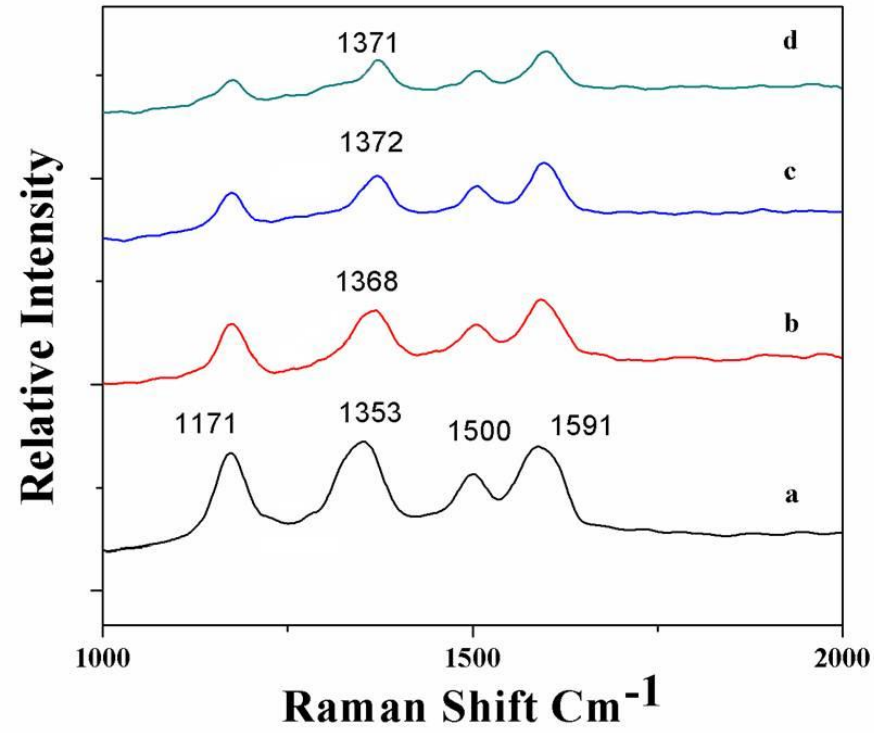

Figure 2: Raman spectra of pure PANI (a), PANI/5 wt% $Ce(NO_3)_3$/3–7 wt% MWCNTs (b–d) nanocomposites

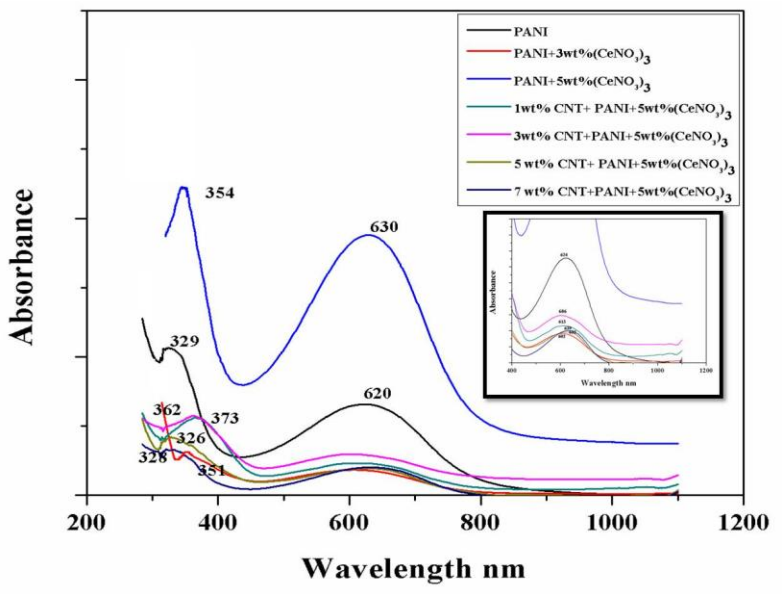

Figure 3: Absorption spectra of pure PANI, PANI/5 wt% $Ce(NO_3)_3$ and PANI/5 wt% $Ce(NO_3)_3$/MWCNTs nanocomposites

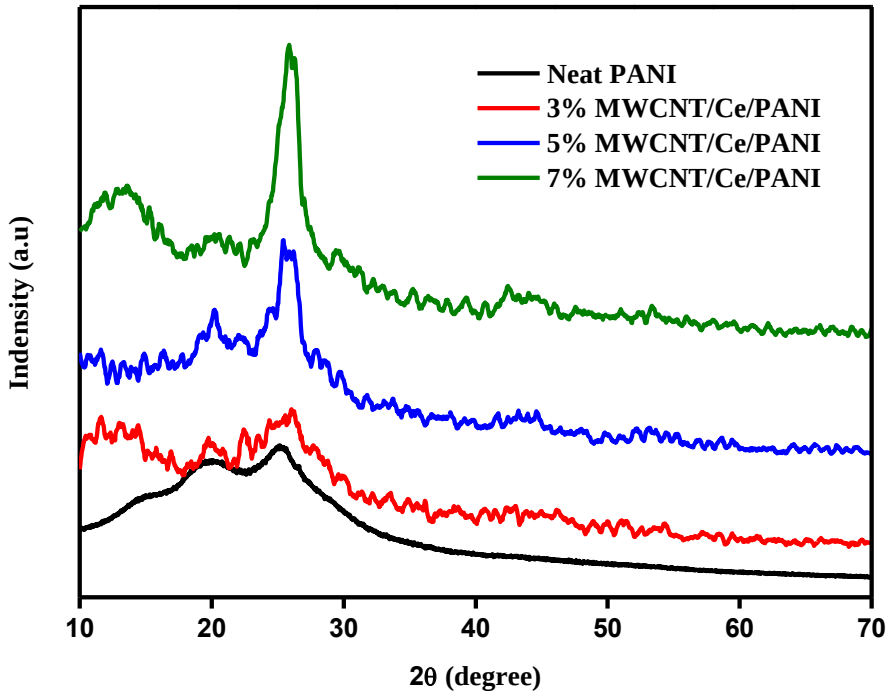

Figure 4: Powder XRD patterns of pure PANI and PANI/5 wt% $Ce(NO_3)_3$/3–7 wt% MWCNTs nanocomposites

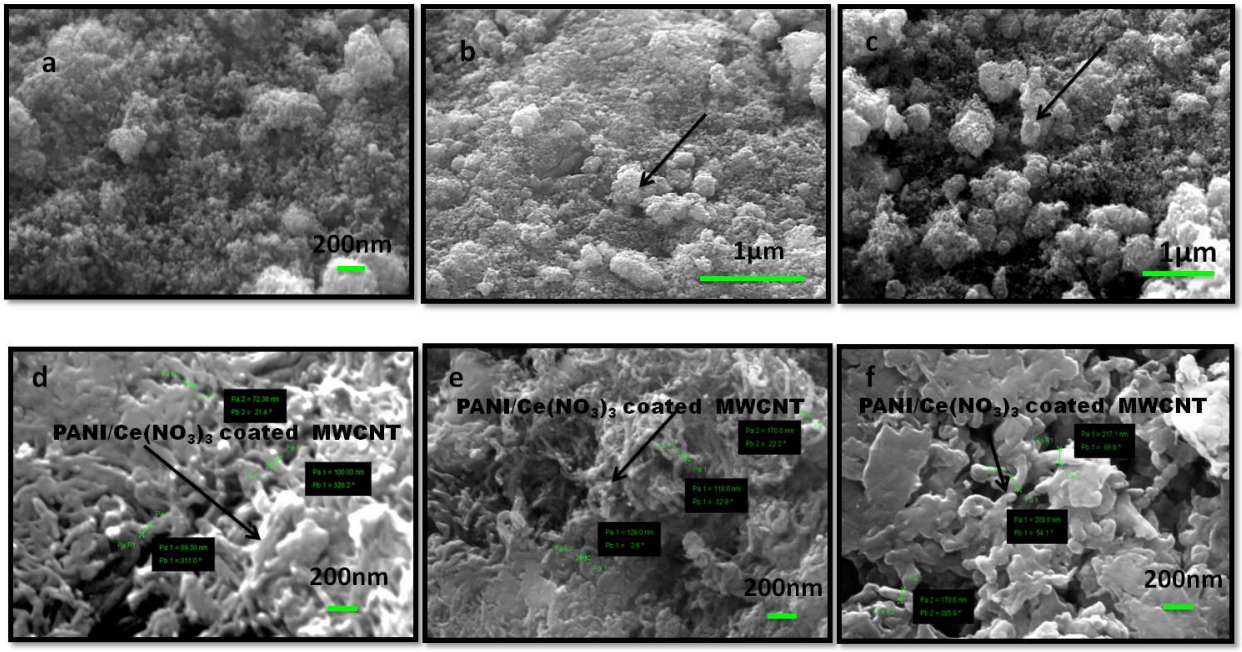

Figure 5: SEM micrographs of PANI, PANI/$Ce(NO_3)_3$ and PANI/$Ce(NO_3)_3$/MWCNTs nanocomposites

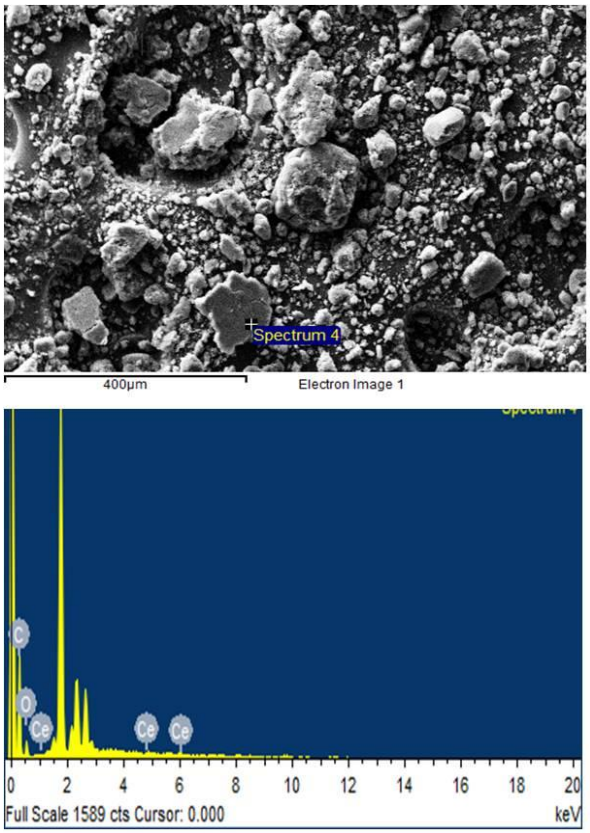

Element	App	Intensity	Weight%	Weight%	Atomic%
	Conc.	Corrn.		Sigma	
C K	1.98	1.4134	67.12	3.24	73.44
O K	0.29	0.4365	32.26	2.99	26.50
Ce L	0.01	0.7676	0.63	2.16	0.06
Totals			100.00		

Figure 6: EDX analysis plot of PANI and PANI/5 wt% $Ce(NO_3)_3$ composites

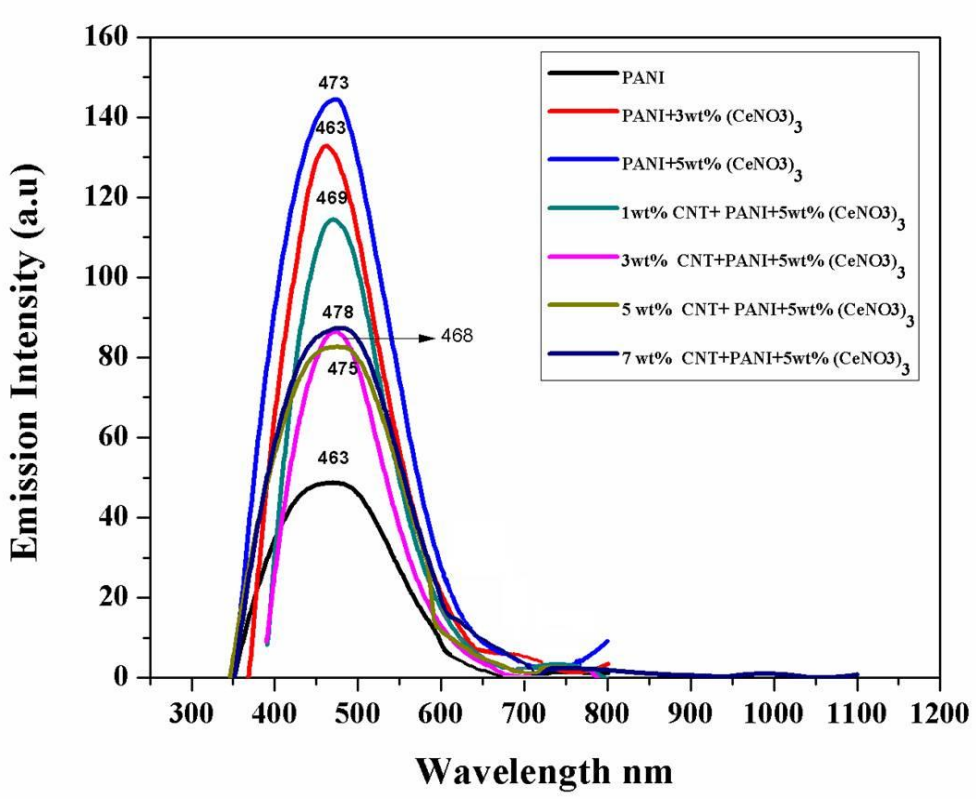

Figure 7: The photoluminescence spectra of pristine PANI, PANI/$Ce(NO_3)_3$ and PANI/$Ce(NO_3)_3$/MWCNTs nanocomposites

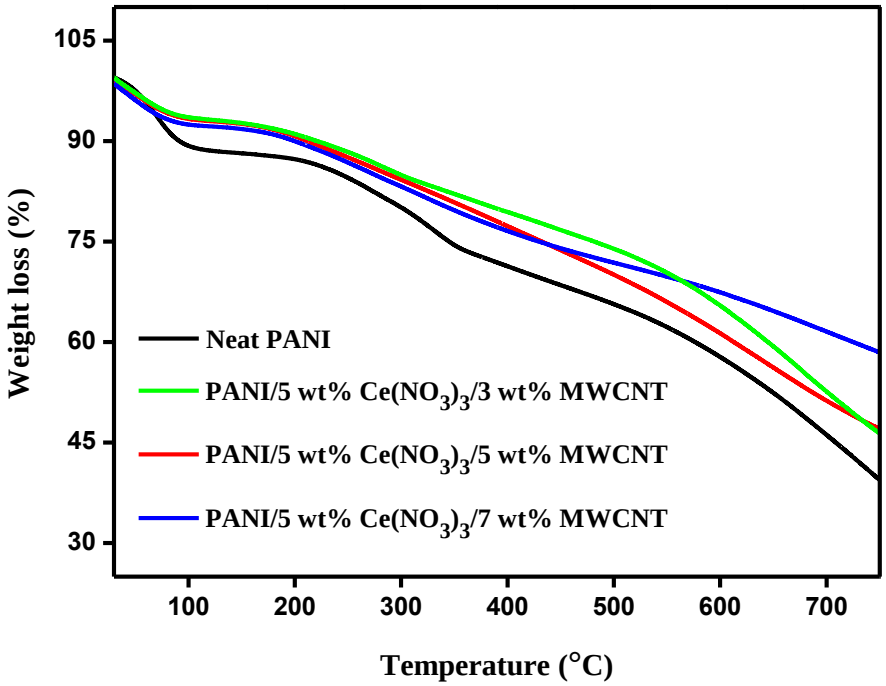

Figure 8: TGA analysis of neat PANI and PANI/5 wt% $Ce(NO_3)_3$/3–7 wt% MWCNTs nanocomposites

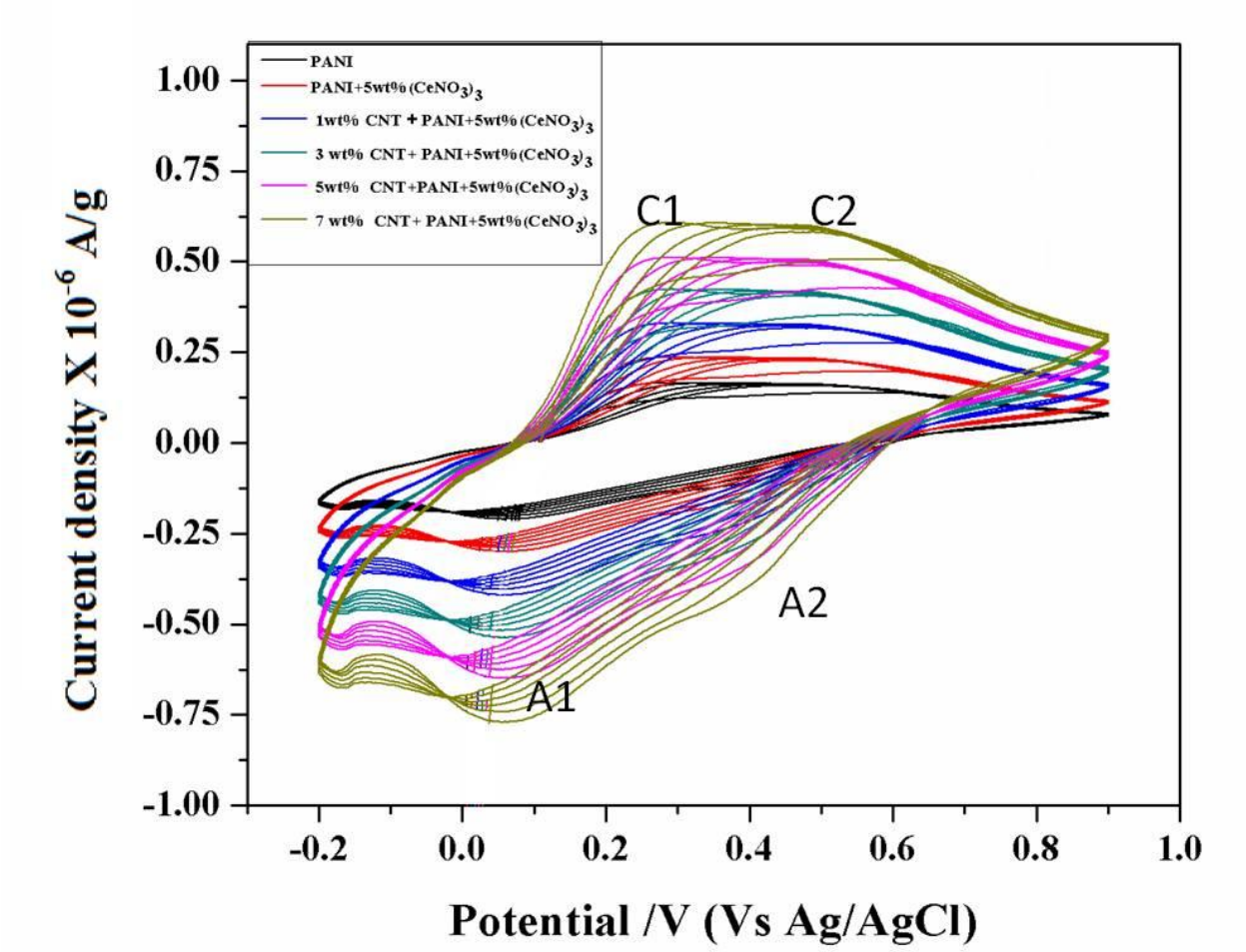

Figure 9: Cyclic voltammograms of pure PANI, PANI/5 wt% $Ce(NO_3)_3$ and PANI/5 wt% $Ce(NO_3)_3$/MWCNTs nanocomposite electrodes at scan rate of 5 mV/s

4. Conclusion

Polymerization of aniline in the presence of MWCNTs leads to the growth of a PANI/5 wt% $Ce(NO_3)_3$/MWCNTs nanocomposites. This is composed of a pure PANI/5 wt% $Ce(NO_3)_3$ matrix and of PANI/5 wt% $Ce(NO_3)_3$ coated MWCNTs. MWCNT coated with PANI/5 wt% $Ce(NO_3)_3$ layers have adopted a more planar conformation of PANI/5 wt% $Ce(NO_3)_3$, thus optimizing the interaction between the PANI/5 wt% $Ce(NO_3)_3$ and the MWCNTs. Furthermore, SEM images show the PANI/5 wt% $Ce(NO_3)_3$ coated MWCNTs formed aligned bundles, which was randomly distributed, thus resulting in a three dimensional network throughout the PANI/$Ce(NO_3)_3$ matrix. The specific capacitance of the nanocomposites attained a highest value of 900 Fg^{-1} with 7 wt% MWCNT doping in PANI/5 wt% $Ce(NO_3)_3$. It is highly remarkable that the luminescent behavior of the PANI/$Ce(NO_3)_3$/ MWCNTs composite is not affected by the presence of MWCNTs. the synergic effect between MWCNT and PANI/5 wt% $Ce(NO_3)_3$ enhanced the specific capacitance of the nanocomposites. The PANI/5 wt% $Ce(NO_3)_3$ nanocomposites with high specific capacitance and PL emission are of great relevance for future technological applications for supercapacitors and improved active components in opto-electronic devices.

Acknowledgements

The authors express their sincere thanks to the Principal and Head of the Department of Chemistry, Presidency College, Chennai, for providing necessary research facilities, and also wish to acknowledge the help of Dr. M. Alagar and Dr. M. Mandhakini, Department of Chemical Engineering, Anna University, Chennai.

Abbreviations

PANI	-	polyaniline
MWCNT	-	multiwalled carbon nanotubes
PL	-	photoluminescence
FT-IR	-	fourier transform-infrared
FE-SEM	-	field emission scanning electron microscopy
UV-Vis	-	ultraviolet-visible
NMP	-	N-methyl-2-pyrrolidone
CV	-	cyclic voltammetry
GC	-	glassy carbon
APS	-	ammonium persulfate
XRD	-	X-ray diffraction
TGA	-	thermogravimetric analysis
wt	-	weight

References

Arbizzani, C., Mastragostino, M., Scrosati, B., Nalwa, H.S. (Ed.). (1997): 'Handbook of Organic Conductive Molecules and Polymers'. Wiley, Chichester, UK 4: 595.

Battacharya, P., Sahoo, S., Das, C.K. (2013): Microwave absorption behaviour of MWCNT based nanocomposites in X-band region. express Polymer Lett., 7: 212–223.

Bian, C., Yu, A., Wu, H. (2009): Fibriform polyaniline/nano-TiO_2 composite as an electrode material for aqueous redox supercapacitors. Electrochem. Commun., 11: 266–269.

Chen, L., Sun, L.J., Luan, F., Liang, Y., Li, Y., Liu, X.X. (2010): Synthesis and pseudocapacitive studies of composite films of polyaniline and manganese oxide nanoparticles. J. Power Sources, 195: 3742–3747.

Chi, C.H., Chien, H.C. (2000): Electrochemical and textural characterization of iridium-doped polyaniline films for electrochemical capacitors. Mater. Chem. Phys., 65: 329–338.

Choi, H.-J., Jeon, I.-Y., Kang, S.-W., Baek, J.-B. (2011): Electrochemical activity of a polyaniline/polyaniline-grafted multiwalled carbon nanotube mixture produced by a simple suspension polymerization. Electrochim. Acta, 56: 10023–10031.

Cochet, M., Maser, W.K., Benito, A.M., Callejas, M.A., Martinez, M.T., Benoit, Schreiber, J., Chauvet, J. (2001): Synthesis of a new polyaniline/nanotube composite: "in-situ" polymerisation and charge transfer through site-selective interaction. Chem. Commun., 16: 1450–1451.

Cong, H.P., Ren, X.C., Wang, P., Yu, S.H. (2013): Flexible graphene–polyaniline composite paper for high-performance supercapacitor. Energy Environ. Sci., 6: 1185–1191.

Conway, B.E. (1999): 'Electrochemical Supercapacitors'. Kluwer Academic/Plenum Publishers, New York.

Conway, B.E. (1991): Transition from "Supercapacitor" to "Battery" Behavior in Electrochemical Energy Storage. J. Electrochem. Soc., 138: 1539–1548.

Fusalba, F., Gouérec, P., Villers, D., Bélanger, D. J. (2001): Electrochemical Characterization of Polyaniline in Nonaqueous Electrolyte and Its Evaluation as Electrode Material for Electrochemical Supercapacitors. Electrochem. Soc., 148: A1–A6.

Ghatak, S., Chakraborty, G., Meikap, A.K., Woods, T., Babu, R., Blau, W.J. (2011): Synthesis and characterization of polyaniline/carbon nanotube composites: J. Appl. Polym. Sci., 119: 1016–1025.

Gopalan, A.I., Lee, K.P., Santhosh, P., Kim, K.S., Nho, Y.C. (2007): Different types of molecular interactions in carbon nanotube/conducting polymer composites – A close analysis. Compos. Sci. Technol., 67: 900–905.

Han, G., Liu, Y., Zhang, L., Kan, E., Zhang, S., Tang, J., Tang, W. (2014): MnO_2 Nanorods Intercalating Graphene Oxide/Polyaniline Ternary Composites for Robust High-Performance Supercapacitors. Sci. Rep., 4: 4824 (1–7).

He, B.L., Zhou, Y.K., Zhou, W.J., Dong, B., Li, H.L. (2004): Preparation and characterization of ruthenium-doped polypyrrole composites for supercapacitor. Mater. Sci. Eng. A, 374: 322–326.

He, H., Zhu, J., Tao, N.J., Nagahara, L.A., Amlani, I., Tsui, R. (2001): A Conducting Polymer Nano junction Switch. J. Am. Chem. Soc., 123:7730–7731.

Huang, J.E., Li, X.H., Xu, J.C., Li, H.L. (2003): Well-dispersed single-walled carbon nanotube/polyaniline composite films, Carbon, 41: 2731–2736.

Hu, Z.A., Xie, Y.L., Wang, Y.X., Mo, L.P., Yang, Y.Y., Zhang, Z.Y. (2009): Polyaniline/SnO_2 nanocomposite for supercapacitor applications. Mater. Chem. Phys.114: 990–995.

Iranagh, S.A., Eskandarian, L., Mohammadi, R. (2013): Synthesis of MnO_2-polyaniline nanofiber composites to produce high conductive polymer. Synth. Met., 172: 49–53.

Jeevananda, T., Siddaramaiah, Kim, N.H., Heo, S.-B., Lee, J.H. (2008): Synthesis and characterization of polyaniline-multiwalled carbon nanotube nanocomposites in the presence of sodium dodecyl sulfate. Polym. Adv. Technol., 19: 1754–1762.

Kotz, R., Carlen, M. (2000): Principles and applications of electrochemical capacitors. Electrochim. Acta, 45: 2483–2498.

Lee, J.H., Park, N., Kim, B.G., Jung, D.S., Im, K., Hur, J., Choi, J.W. (2013): Restacking-Inhibited 3D Reduced Graphene Oxide for High Performance Supercapacitor Electrodes. ACS Nano, 7: 9366–9374.

Li, L., Loveday, D.C., Mudigonda, D.S.K., Ferraris, J.P., Cantero, I. (2002): Effect of Electrolytes on Performance of Electrochemical Capacitors Based on Poly[3-(3,4- difluorophenyl)thiophene]. J. Electrochem. Soc., 149: A1201–1207.

Li, Q., Wang, Z.L., Li, G.R., Guo, R., Ding, L.X., Tong, Y.X. (2012): Design and Synthesis of MnO_2/Mn/MnO_2 Sandwich-Structured Nanotube Arrays with High Supercapacitive Performance for Electrochemical Energy Storage: Nano Lett., 12: 3803–3807.

-Markovic, M.G., Matisons, J.G., Cervini, R., Simon, G.P., Fredericks, P.M. (2006): Synthesis of New olyaniline/ Nanotube Composites Using Ultrasonically Initiated Emulsion Polymerization. Chem. Mater., 18: 6258–6265.

Nayak, G.C., Rajasekar, R., Sahoo, S., Das, C.K., Saxena, A.K., Ranjan, A. (2011): Effect of polyphosphazene and modified carbon nanotubes on the morphological and thermo- mechanical properties of polyphenylene sulfide and liquid crystalline polymer blend system. J. Mater. Science, 46: 7672–7680.

Ni, W., Wang, D., Huang, Z. (2010): J. Zhao, G. Cui, Fabrication of nanocomposite electrode with MnO_2 nanoparticles distributed in polyaniline for electrochemical capacitors. Mater. Chem. Phys., 124: 1151–1154.

Otero, T.F. (1999): Conducting polymers as positive electrodes in rechargeable lithium-ion batteries. J. Power Sources, 81–82: 838–841.

Ozkazanc, E., Zor, S., Ozkazanc, H., Guney, H.Y., Abaci, U. (2012): Synthesis, characterization and dielectric behavior of (ES)-form polyaniline/cerium(III)-nitrate-hexahydrate composites. Mater. Chem. Phys., 133: 356–362.

Patil, D.S., Shaikh, J.S., Dalavi, D.S., Karanjkar, M.M., Devan, R.S. Ma, Y.R., Patil, P.S. (2011): An Mn Doped Polyaniline Electrode for Electrochemical Supercapacitor. J. Electrochem. Soc., 158: A653–A657.

Reisfeld, R., Minti, H., Patra, A., Ganguli, D., Gaft, M. (1998): Spectroscopic properties of cerium in glasses and their comparison with crystals. Spectrochim. Acta A, 54: 2143–2150.

Ryu, K.S., Kim, K.M., Park, N.G., Park, Y.J., Chang, S.H. (2002): Symmetric redox supercapacitor with conducting polyaniline electrodes. J. Power Sources, 103: 305–309.

Rudge, A., Davey, J., Raistrick, I., Gottesfeld, S., Ferraris, J.P. (1994): Conducting polymers as active materials in electrochemical capacitors, J Power Sources, 47: 89–107.

Saini, P., Choudhary, V., Sinha, B.P., Mathur, R.B., Dhawan, S.K. (2009): Polyaniline–MWCNT nanocomposites for microwave absorption and EMI shielding. Mater. Chem. Phys., 113: 919–926.

Wang, Y.-G., Li, H.Q., Xia, Y.Y. (2006): Ordered Whiskerlike Polyaniline Grown on the Surface of Mesoporous Carbon and Its Electrochemical Capacitance Performance. Adv. Mater., 18: 2619–2623.

Wang, G., Tang, Q., Bao, H., Li, X., Wang, G. (2013): Synthesis of hierarchical sulfonated graphene/MnO_2/polyaniline ternary composite and its improved electrochemical performance. J. Power Sources, 241: 231–238.

Wang, X., Zhang, Y., Zhi, C., Wang, X., Tang, D., Xu, Y., Weng, Q., Jiang, X., Mitome, M., Golberg, D., Bando, Y. (2013): Three-dimensional strutted graphene grown by substrate-free sugar blowing for high-power-density supercapacitors. Nat. Commun., 4:2905 (1–8).

Xie, S., Gan, M., Ma, L., Li, Z., Yan, J., Yin, H., Shen, X., Xu, F., Zheng, J., Zhang, J., Hu, J. (2014): Synthesis of polyaniline-titania nanotube arrays hybrid composite *via* self- assembling and graft polymerization for super-capacitor application. Electrochim. Acta, 120: 408–415.

Xu, C.L., Bao, S.J., Kong, L.B., Li, H., Li, H.L. (2006): Highly ordered MnO_2 nanowire array thin films on Ti/Si substrate as an electrode for electrochemical capacitor: J. Solid State Chem., 179: 1351–1355.

Yang, J., Wang, X., Wang, X., Jia, R., J. Huang, R. (2010): Preparation of highly conductive CNTs/polyaniline composites through plasma pretreating and in-situ polymerization. J. Phys. Chem. Solids, 71: 448–452.

Yuan, C., Yang, L., Hou, L., Li, J., Sun, Y., Zhang, X., Shen, L., Lu, X., Xiong, S., Lou, X.W. (2012): Flexible Hybrid Paper Made of Monolayer Co_3O_4 Microsphere Arrays on rGO/CNTs and Their Application in Electrochemical Capacitors. Adv. Funct. Mater., 22: 2560–2566.

Yu, G., Hu, L., Liu, N., Wang, H., Vosgueritchian, M., Yang, Y., Cui, Y., Bao, Z. (2011): Enhancing the Supercapacitor Performance of Graphene/MnO_2 Nanostructured Electrodes by Conductive Wrapping. Nano Lett., 11: 4438–4442.

Yu, G., Hu, L., Vosgueritchian, M., Wang, H., Xie, X., Mcdonough, J.R., Cui, X., Cui, Y., Bao, Z. (2011): Solution-Processed Graphene/MnO_2 Nanostructured Textiles for High- Performance Electrochemical Capacitors. Nano Lett., 11: 2905–2911.

Zengin, H., Zhou, W., Jin, J., Czerw, R., Smith Jr., D.W., Echegoyen, L., Carroll, D.L., Foulger, S.H., Ballato, J. (2002): Carbon Nanotube Doped Polyaniline. Adv. Mater., 14: 1480–1483.